Electrocatalysis

Deutsche Ausgabe: DOI: 10.1002/ange.201602851
Internationale Ausgabe: DOI: 10.1002/anie.201602851

Enhanced Intrinsic Catalytic Activity of λ-MnO_2 by Electrochemical Tuning and Oxygen Vacancy Generation

Sanghan Lee, Gyutae Nam, Jie Sun, Jang-Soo Lee, Hyun-Wook Lee, Wei Chen, Jaephil Cho, and Yi Cui**

Abstract: *Chemically prepared λ-MnO_2 has not been intensively studied as a material for metal–air batteries, fuel cells, or supercapacitors because of their relatively poor electrochemical properties compared to α- and δ-MnO_2. Herein, through the electrochemical removal of lithium from $LiMn_2O_4$, highly crystalline λ-MnO_2 was prepared as an efficient electrocatalyst for the oxygen reduction reaction (ORR). The ORR activity of the material was further improved by introducing oxygen vacancies (OVs) that could be achieved by increasing the calcination temperature during $LiMn_2O_4$ synthesis; a concentration of oxygen vacancies in $LiMn_2O_4$ could be characterized by its voltage profile as the cathode in a lithiun–metal half-cell. λ-MnO_{2-z} prepared with the highest OV exhibited the highest diffusion-limited ORR current (5.5 mA cm^{-2}) among a series of λ-MnO_{2-z} electrocatalysts. Furthermore, the number of transferred electrons (n) involved in the ORR was >3.8, indicating a dominant quasi-4-electron pathway. Interestingly, the catalytic performances of the samples were not a function of their surface areas, and instead depended on the concentration of OVs, indicating enhancement in the intrinsic catalytic activity of λ-MnO_2 by the generation of OVs. This study demonstrates that differences in the electrochemical behavior of λ-MnO_2 depend on the preparation method and provides a mechanism for a unique catalytic behavior of cubic λ-MnO_2.*

The electrochemical oxygen reduction reaction (ORR) has been extensively studied in recent decades to enhance its sluggish kinetics for application in a variety of devices for energy storage and conversion, such as metal–air batteries and fuel cells.[1] Platinum-based materials are the best electrocatalysts for ORR in both acidic and alkaline conditions. However, these materials suffer from high cost and low stability when used for metal–air batteries and fuel cells.[2] As an alternative to noble metals, manganese dioxide (MnO_2) is one of the more attractive materials for applications in catalysis, energy storage, and energy conversion, because it is abundant, low-cost, environmentally friendly, and displays considerable electrochemical properties.[3] MnO_2 has different crystal structures (such as the α, β, γ, δ, and λ forms) depending on synthesis conditions. The electrochemical properties of MnO_2 largely depend on its crystal structure.[4] Of the variety of MnO_2 materials, α- and δ-MnO_2 have been highlighted because of their excellent electrochemical performance in various applications.[5] For example, electrochemical performance increases in the order of β-MnO_2 < λ-MnO_2 < γ-MnO_2 < δ-MnO_2 ≈ α-MnO_2 in the fields of both metal–air batteries and supercapacitors.[4b,c] However, those comparisons might be unfair for λ-MnO_2, which is a metastable form of MnO_2, because the material is prepared by acidic leaching for the removal of lithium from $LiMn_2O_4$.[6] MnO_2 is unstable under acidic conditions, and material degradation during synthesis is unavoidable. Therefore, high quality λ-MnO_2 is needed. Meanwhile, MnO_2 catalysts have shown lower intrinsic activity than noble-metal-based catalysts because of their poor affinity for O_2 adsorption and low conductivity, leading to larger overpotentials and smaller current densities.[7] Recently, the electrochemical performance of MnO_2 was shown to be enhanced by generating OVs.[8]

Herein, λ-MnO_2 was studied as an electrocatalyst for the ORR; λ-MnO_{2-z} was first electrochemically synthesized using $LiMn_2O_{4-z}$ as a precursor, which allows the product to maintain high crystallinity during the preparation. Such a method of electrochemical tuning of catalysts was recently developed by some of us on Li-tuning of MoS_2 for the hydrogen evolution reaction, Li metal oxide intercalation compounds, olivine oxides, and conversion oxides for oxygen evolution.[9] A strategy is also demonstrated for enhancing the intrinsic catalytic activity of λ-MnO_{2-z} by introducing more oxygen deficiencies (z) through high-temperature calcination. Furthermore, a mechanism was proposed for the acceleration of one-electron transfer from the catalyst to the adsorbed O_2 caused by the instability of Mn^{3+} in a cubic crystal structure.

$LiMn_2O_4$ was prepared in a conventional solid-state reaction at 700 °C for 12 h in an O_2 atmosphere. To introduce different O_2 deficiencies to the samples, the particles were then fired at different temperatures of 750 °C, 900 °C, and 1050 °C in air. The resulting materials were used to fabricate three kinds of λ-MnO_{2-z} catalysts by electrochemical delithiation (denoted as 750MO, 900MO, and 1050MO, corresponding to the firing temperature used during synthesis), which were evaluated in this study. In addition, a chemically delithiated sample (denoted 1050CDMO) was prepared to investigate the differences between electrochemical and chemical preparations of λ-MnO_{2-z}.

[*] Dr. S. Lee, Dr. J. Sun, Dr. J. Lee, Dr. H. Lee, Dr. W. Chen, Prof. Y. Cui
Department of Materials Science and Engineering
Stanford University
Stanford, CA 94305 (USA)
E-mail: yicui@stanford.edu
Dr. S. Lee, G. Nam, Dr. J. Lee, Prof. J. Cho
Department of Energy Engineering and
School of Energy and Chemical Engineering
Ulsan National Institute of Science and Technology (UNIST)
689-798, Ulsan (Republic of Korea)
E-mail: jpcho@unist.ac.kr

Supporting information for this article can be found under: http://dx.doi.org/10.1002/anie.201602851.

The use of a higher temperature for the solid-state reaction for metal oxide preparation accelerates particle growth, leading to a decrease in the surface area. The morphologies of electrochemically delithiated 750MO, 900MO, and 1050MO samples showed gradual increases in particle size with increased firing temperature, while no changes were observed with electrochemical delithiation (Figures 1; Supporting Information, Figure S1). Ideally, obtaining a high-surface-area material is an important requirement for catalysts used in energy conversion devices.

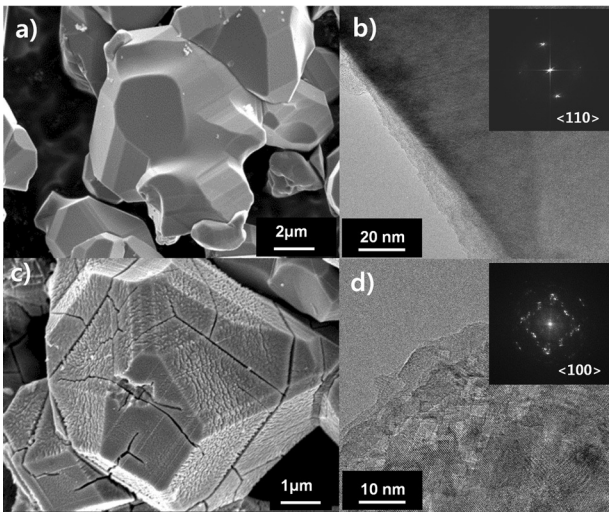

Figure 1. Characterization of the samples. SEM and TEM images of electrochemically synthesized λ-MnO_2. a) SEM image of 1050MO and chemically prepared λ-MnO_2. b) TEM image of 1050MO. c) SEM image of 1050CDMO. d) TEM image of 1050CDMO. The diffraction pattern of 1050MO exhibits a single crystal structure, while that of 1050CDMO shows a polycrystalline structure in the insets to (b) and (d).

In this regard, 750MO should have exhibited the best catalytic performance among the samples. In addition, remarkable differences in morphology between the chemically delithiated sample (1050CDMO) and the electrochemically prepared one (1050MO) were observed (Figures 1 a, 1 c, and S2). The 1050CDMO sample had a rough surface with micro-cracks, whereas 1050MO exhibited no change from its pristine morphology before electrochemical delithiation. For structural details, Figures 1 b and 1 d show high-resolution transmission electron microscopy (TEM) images of primary particles from the samples. Primary particles of 1050MO exhibited a single crystalline structure, whereas 1050CDMO had a polycrystalline structure. This might be the result of the different reaction times used for electrochemical and chemical delithiation. Chemical delithiation (1050CDMO) reached near completion in only a few minutes. This rapid delithiation might have caused significant lattice strain during the process because of the difference in lattice parameters between $LiMn_2O_4$ (8.238 Å, JCPDS: #35-0782) and λ-MnO_2 (8.029 Å JCPDS: #44-0992), resulting in the pulverization of single crystals. On the other hand, electrochemical delithiation (1050MO) was conducted in a Li metal half-cell at a very slow charging rate of 0.05 C, corresponding to a controllable reaction time of 20 h. This slow process could be the reason why 1050MO exhibited a highly crystalline morphology. The remarkable difference between the chemically and electrochemically prepared λ-MnO_2 results in their significantly different electrocatalytic performances.

On the other hand, great efforts have been made to elucidate the effect of O_2 deficiency on catalytic performance. Chen et al. found that the catalytic activity of β-MnO_2 was enhanced by generating an O_2 deficiency.[8d] The oxygen deficiency of $LiMn_2O_4$ as a cathode material for lithium ion batteries has been intensively studied over the last two decades because it plays a key role in determining the electrochemical performance, especially cycle performance.[10] Gao and Dahn suggested the use of a 3.2-V discharge (lithiation) plateau as an indicator for detecting O deficiencies,[11] while Masaki et al. reported a linear relationship between the capacity at ≈3.2 V and z in $LiMn_2O_{4-z}$.[12] Based on these findings and the first discharge curves of the sample (Figure 2 a), the O_2 deficiency, z, of the samples was calculated as shown in Figure 2 b. As the calcination temperature increased, a greater O_2 deficiency was generated. X-ray diffraction patterns of the samples are shown in Figure S1. For samples prior to delithiation, all of the diffraction peaks could be assigned to the cubic spinel phase of $LiMn_2O_4$ (space group $Fd\bar{3}m$). For samples after electrochemical and chemical delithiation, all of the diffraction peaks could also be assigned to the cubic spinel phase of λ-MnO_2 (space group $Fd\bar{3}m$). A shift toward a higher angle was observed with all samples and

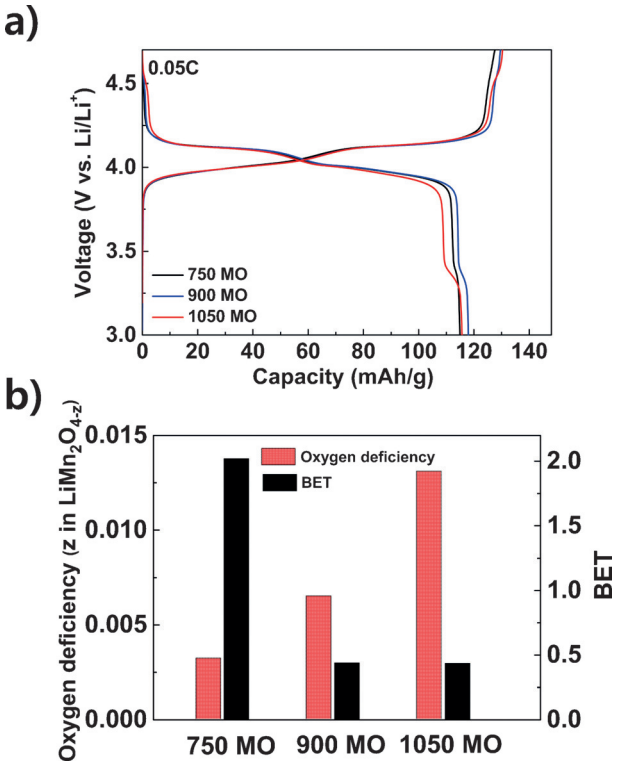

Figure 2. Characterization of the samples. a) The first charge and discharge curves of the samples in Li metal half-cells. The ≈3.2 V capacity is proportional to the oxygen deficiency. b) Oxygen deficiency, z, and BET surface area of the samples. BET surface area of 1050CDMO was ≈0.48 $m^2 g^{-1}$.

was due to an increase in the average oxidation state of the Mn ion of Mn^{3+} to Mn^{4+}, which was accompanied by Li extraction.

Catalytic ORR activities of the 1050MO/C at room temperature were characterized with rotating disk electrode (RDE) measurement in O_2-saturated electrolyte solution (0.1M KOH) on a glassy carbon electrode. Typical linear sweep voltammetry (LSV) curves at a potential scan rate of 10 mV S^{-1} were obtained after stabilization of the working electrode by several cyclic voltammetry (CV) cycles as shown in Figure 3. The same LSV curves for all of the samples were obtained in N_2-saturated solution after completion of tests in O_2-saturated solution to correct for the capacitive current. Therefore, the LSV curves in Figure 3a directly reflect the ORR activities of the samples. The electrochemically prepared 1050MO showed much higher ORR activity in terms of limiting current density than the chemically prepared 1050CDMO, and the difference between the two could be determined by their morphologies. The surface of the primary particles of 1050CDMO was fragmented into tiny particles during preparation, as indicated by the many visible cracks on the surface (Figures 1 and S2). These boundary interfaces resisted the passage of electrons such that the active sites of 1050CDMO for the ORR might be reduced compared with those of 1050MO. Figure 3b shows a Koutecky–Levich (K-L) plot constructed from rotation speed-dependent current to verify the ORR kinetics. Figure 3c also shows the number of transferred electrons, n, during the ORR as a function of applied voltage. Values of $n = 3.2$ and $n = 3.8$ were obtained for 1050CDMO and 1050MO, respectively, indicating a remarkable difference in ORR activity between synthetic methods. The ORR activities of MnO_2 depended strongly on its crystal structure, following the performance sequence of β-$MnO_2 < \lambda$-$MnO_2 < \gamma$-$MnO_2 < \alpha$-$MnO_2 \approx \delta$-MnO_2.[3k,4b] However, all of the λ-MnO_2 materials reported in literature were chemically prepared, which might have caused the relatively poor performance of λ-MnO_2. In this work, highly crystalline λ-MnO_{2-z} was prepared by an electrochemical method and demonstrated a high catalytic activity for the ORR with a number of transferred electrons of ≈ 3.8, which is comparable to that of α-MnO_2 ($n \approx 3.8$). α-MnO_2 is one of the best catalysts for the ORR among the different types of MnO_2.

Three other samples (750MO, 900MO, and 1050MO) were prepared using the electrochemical delithiation method. These samples were studied to elucidate the relationship between OV amount and ORR activity. Figure 4 shows typical CV curves of the samples in an N_2-saturated electrolyte, indicating electrochemical double layer capacitance (EDLC). Small oxidation and reduction peaks were observed near −0.07 V and 0.02 V, respectively, which could be correlated to the $Mn^{3+/4+}$ redox couple. This phenomenon will be discussed later in the text. By plotting the current at 0.2 V vs. Hg/HgO as a function of scan rate, the EDLCs of the samples were calculated (Figure S4). As the calcination temperature of $LiMn_2O_{4-z}$ preparation increased, the sample exhibited a lower capacitance, indicating a decrease in electrochemically active surface area, which was caused by larger particles at higher temperature. The EDLCs of the working electrodes for 1050MO, 900MO, and 750MO were 11.4, 11.1, and 119.6 mF cm^{-2}, respectively. 750MO exhibited the highest capacitance because of the small particle size. It is believed that not all of the electrochemical surface area based on the EDLC calculation was involved in the ORR, because not all the electrochemical surfaces offers a three-phase zone of gas, liquid, and solid for the ORR to proceed. However, samples with a larger surface area would still be expected to contribute more surface area for ORR. 750MO clearly had a much larger surface area than the other samples based on its high EDLC and BET surface. According to these observations, 750MO should have exhibited the best performance among the samples. However, as shown in

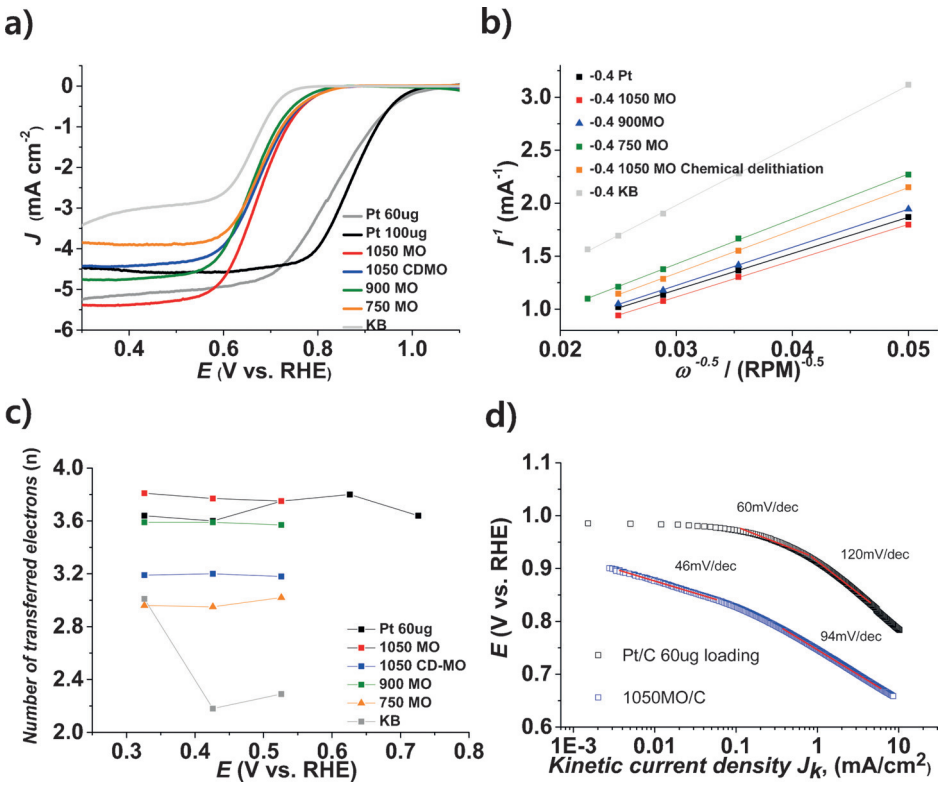

Figure 3. Electrochemical properties of the samples in 0.1M KOH aqueous solution saturated with O_2. a) Steady-state LSV curves of the samples. b) Koutecky–Levich plot at 0.526 V vs. RHE. c) Electron transfer number (n) as a function of applied voltage. d) Mass-transport-corrected Tafel plot for ORR on 1050MO/C and Pt/C electrocatalysts.

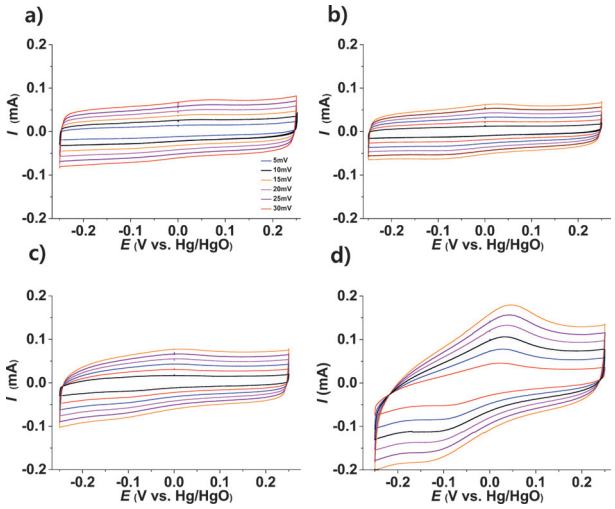

Figure 4. Cyclic voltammograms in 0.1M KOH aqueous solution saturated with N_2. a) 1050MO. b) 1050CDMO. c) 900MO. d) 750MO. The electrochemical double-layer capacitance (EDLC) of the samples was measured by performing CV scans at various scan rates (30, 25, 20, 15, 10, and 5 $mV s^{-1}$) in a potential range of 0.25 to −0.25 V vs. Hg/Hg.

Figure 3a, the catalytic activities of 1050MO, 900MO, and 750MO did not exhibit performances that were dependent on surface area (Figure 3). In Figure 3a, 1050MO, which had the smallest surface area, displayed the best performance, and its limiting current was 5.5 $mA cm^{-2}$, which is comparable to that of Pt/C. For the number of transferred electrons involved in the ORR, 1050MO showed a dominant quasi-4-electron reduction pathway, while 900MO and 750MO exhibited much lower n values of ≈3.6 and ≈3.0 over the potential range of 0.526–0.326 V, respectively. This performance order was the reverse of the sequence of increasing surface area, but followed the sequence of increasing OV. These results suggest that the catalytic activity per unit area of λ-MnO_{2-z} can be improved by introducing OVs that produce an improvement in the intrinsic catalytic properties.

As the OV increased, the sample exhibited a larger limiting current. However, no significant changes in ORR onset potential and half-wave potential were observed. Moreover, mass-transfer-corrected Tafel slopes for variable λ-MnO_{2-z} showed two distinct slopes of 45 and 95 $mV dec^{-1}$ (Figures 3d and S8), but the variation in the slopes among the samples was very small, indicating that they followed similar activation processes for the ORR. Furthermore, different Tafel slopes from the Pt/C electrocatalysts indicated that the λ-MnO_{2-z} series was not controlled by superoxide formation through a one-electron transfer process.[13] The rate-determining step for λ-MnO_{2-z} might be O_2 adsorption or the formation of intermediates such as OOH^- and OH^-. Therefore, the enhancement in limiting current density was mainly attributed to an increase in the number of ORR active sites, which increases the O_2 adsorption energy or electronic conductivity at grain boundaries.[8a]

Interestingly, the ORR onset potential of the samples in O_2-saturated electrolyte was almost the same as the reduction potential of Mn^{4+} in N_2-saturated electrolyte (Figure 5a), which is in an agreement with the mechanism.[14] All of the λ-MnO_{2-z} samples displayed characteristic peaks for the $Mn^{3+/4+}$ redox couple. 750MO exhibited the highest peak intensity owing to its high surface area. For the metal oxide catalyst, the reduction of adsorbed O_2 to adsorbed peroxide is likely the rate-determining step,[8d] and an octahedral site cation, which has a d^4 configuration with one electron in the antibonding e_g orbital, displayed a high activity for the ORR irrespective of the crystallographic structure of the catalyst.[15] Accordingly, 750MO would be expected to be well-suited for the ORR, because it displayed the highest peak current for Mn^{4+} reduction. Nevertheless, 1050MO exhibited the best ORR activity, implying that either 1) the rate-determining step for cubic λ-MnO_2 was not a one-electron pathway, or 2) the one-electron transfer of cubic λ-MnO_2 was much faster than that of other phases of MnO_2, as evidenced by a difference in the Tafel slope from that of Pt-based catalysts (Figure 3d).

The ORR mechanism for MnO_2 is still not completely understood. Brenet proposed that the electrochemical reduction of O_2 occurs through the oxidation of Mn^{III}, which is cyclically produced by the reduction of Mn^{IV}.[14]

$$Mn^{4+} + e \rightarrow Mn^{3+} \quad \text{(fast)} \qquad (1)$$

$$Mn^{3+} + O_2(ads) \rightarrow Mn^{4+} + O_2^-(ads) \quad \text{(slow)} \qquad (2)$$

An acceleration of one-electron transfer processes by cubic λ-MnO_{2-z} was expected, because of its unique crystal

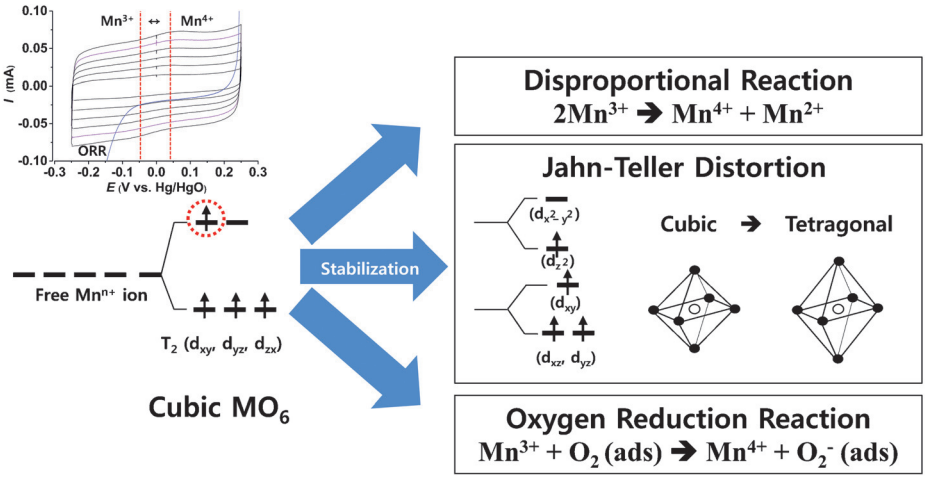

Figure 5. LSV curve and CV curves of 1050MO in O_2-saturated solution and N_2-saturated solution, respectively, and a proposed mechanism for the catalytic activity of spinel λ-MnO_2.

structure, which is different from that of the other phases of MnO_2. The crystal structure of λ-MnO_2 was cubic. Its basic structural unit was an octahedron of MnO_6 with a formal oxidation state of +4. In a cubic crystal structure, Mn^{3+} in the MO_6 octahedron was unstable, because of unpaired single electrons at a high energy level in the e_g band (Mn^{3+}, t_{2g}^3, e_g^1). Three possible mechanisms can induce self-stabilization. The first was Jahn–Teller distortion, which can easily occur when the average oxidation state is lower than 3.5 in a single crystal particle. However, it is difficult to transform the entire crystal structure to that of a single crystal through the small amount of localized Mn^{3+} at the surface. The second mechanism is a disproportional reaction, which can proceed as $2Mn^{3+} \rightarrow Mn^{4+} + Mn^{2+}$. Mn^{2+} can be dissolved into the electrolyte, resulting in material loss. However, 1050MO exhibited better durability than Pt-based catalysts, indicating that this reaction is not significant (Figure S9). The third mechanism was the ORR. In an ORR potential range, adsorbed O_2 is likely reduced and Mn^{3+} is likely to be stabilized. This might have caused the one-electron transfer from Mn^{3+} to adsorbed O_2 to have a high probability compared to other reactions. Therefore, the acceleration of the one-electron transfer process in cubic λ-MnO_{2-z} was likely caused by the self-stabilization of the cubic crystal structure of Mn^{3+}.

We generated a zinc–air battery with a desired electrocatalyst coated on the air electrode and Zn plate as the anode electrode. All of the cathode materials were coated on the surface of the bare air electrode to prepare a 2-layer cathode material for the zinc–air battery test. Figure S12 presents the polarization curves of different cathode material. Although 1050MO exhibits lower on-set potential than the 20% Pt/C catalyst in half-cell test using the RRDE method, 1050MO has a similar voltage vs. current profile to platinum-based electrocatalysts.

Electrochemically prepared λ-MnO_{2-z} was shown to exhibit a significantly improved catalytic performance over chemically prepared samples, and its catalytic activity was enhanced by introducing more OVs. That the ORR onset potential was well matched with the reduction potential of Mn^{4+} was confirmed, but the higher current for Mn^{4+} reduction, which was enabled by the large surface area, did not lead to a higher current density for the ORR. Therefore, the rate-determining step of the reaction was different than that for other manganese oxides for which the ORR proceeds as a one-electron transfer process. It was proposed that the kinetics of the one-electron transfer for λ-MnO_2 was enhanced by the instability of Mn^{3+} in its cubic crystal structure in which Mn^{3+} can lose one electron to adsorbed O_2 for self-stabilization. As a result, O_2 adsorption was likely the rate-determining step, and the O_2 adsorption energy, which was enhanced by introducing OVs, played an important role in enhancing the electrochemical performance of the material. Overall, the results provide insight into the mechanism of the catalytic activity of MnO_2. In addition, the electrochemical behavior of chemically prepared λ-MnO_2 was extensively studied, showing that the method leads to morphology and structure degradations in the material. However, electrochemically prepared λ-MnO_2 has seldom been investigated in prior work. In this work, the difference between electrochemically and chemically prepared λ-MnO_2 was demonstrated, indicating the necessity of an in-depth exploration of cubic λ-MnO_2 to investigate its intrinsic electrochemical properties.

Acknowledgements

This work was supported by the BK21 Plus Program (META-material-based Energy Harvest and Storage Technologies, 10Z20130011057) funded by the Ministry of Education (MOE, Korea) and National Research Foundation of Korea (NRF). The authors acknowledge the support from Stanford GCEP.

Keywords: electrocatalysts · manganese · oxides · oxygen reduction reaction · zinc–air battery

How to cite: *Angew. Chem. Int. Ed.* **2016**, *55*, 8599–8604
Angew. Chem. **2016**, *128*, 8741–8746

[1] a) A. A. Gewirth, M. S. Thorum, *Inorg. Chem.* **2010**, *49*, 3557–3566; b) M. Armand, J. M. Tarascon, *Nature* **2008**, *451*, 652–657; c) J. Lee, S. T. Kim, R. Cao, N. Choi, M. Liu, K. T. Lee, J. Cho, *Adv. Energy Mater.* **2011**, *1*, 34–50; d) P. G. Bruce, S. A. Freunberger, L. J. Hardwick, J. M. Tarascon, *Nat. Mater.* **2012**, *11*, 19–29; e) J. Duan, S. Chen, M. Jaroniec, S. Z. Qiao, *ACS Catal.* **2015**, *5*, 5207–5234.

[2] a) V. Stamenkovic, B. S. Mun, K. J. Mayrhofer, P. N. Ross, N. M. Markovic, J. Rossmeisl, J. Greeley, J. K. Norskov, *Angew. Chem. Int. Ed.* **2006**, *45*, 2897–2901; *Angew. Chem.* **2006**, *118*, 2963–2967; b) R. Srivastava, P. Mani, N. Hahn, P. Strasser, *Angew. Chem. Int. Ed.* **2007**, *46*, 8988–8991; *Angew. Chem.* **2007**, *119*, 9146–9149; c) F. Cheng, J. Chen, *Chem. Soc. Rev.* **2012**, *41*, 2172–2192; d) R. Zhou, S. Z. Qiao, *Chem. Commun.* **2015**, *51*, 7516–7519; e) J. Liang, R. F. Zhou, X. M. Chen, Y. H. Tang, S. Z. Qiao, *Adv. Mater.* **2014**, *26*, 6074–6079.

[3] a) T. Zhang, F. Cheng, J. Du, Y. Hu, J. Chen, *Adv. Energy Mater.* **2015**, *5*, 1400654; b) M. S. El-Deab, T. Ohsaka, *Angew. Chem. Int. Ed.* **2006**, *45*, 5963–5966; *Angew. Chem.* **2006**, *118*, 6109–6112; c) F. Cheng, J. Shen, B. Peng, Y. Pan, Z. Tao, J. Chen, *Nat. Chem.* **2011**, *3*, 79–84; d) K. L. Pickrahn, S. W. Park, Y. Gorlin, H. Lee, T. F. Jaramillo, S. F. Bent, *Adv. Energy Mater.* **2012**, *2*, 1269–1277; e) Y. Gorlin, T. F. Jaramillo, *J. Am. Chem. Soc.* **2010**, *132*, 13612–13614; f) A. Débart, A. J. Paterson, J. Bao, P. G. Bruce, *Angew. Chem. Int. Ed.* **2008**, *47*, 4521–4524; *Angew. Chem.* **2008**, *120*, 4597–4600; g) I. Roche, K. Scott, *J. Appl. Electrochem.* **2009**, *39*, 197–204; h) G. Yu, L. Hu, N. Liu, H. Wang, M. Vosgueritchian, Y. Yang, Y. Cui, Z. Bao, *Nano Lett.* **2011**, *11*, 4438–4442; i) J. Yan, Z. Fan, T. Wei, W. Qian, M. Zhang, F. Wei, *Carbon* **2010**, *48*, 3825–3833; j) F. H. B. Lima, M. L. Calegaro, E. A. Ticianelli, *J. Electroanal. Chem.* **2006**, *590*, 152–160.

[4] a) M. M. Thackeray, *Prog. Solid State Chem.* **1997**, *25*, 1–71; b) Y. L. Cao, H. X. Yang, X. P. Ai, L. F. Xiao, *J. Electroanal. Chem.* **2003**, *557*, 127–134; c) S. Devaraj, N. Munichandraiah, *J. Phys. Chem. C* **2008**, *112*, 4406–4417; d) Y. Gorlin, D. Nordlund, T. F. Jaramillo, *ECS Trans.* **2013**, *58*, 735–750; e) Y. Gorlin, T. F. Jaramillo, *J. Electrochem. Soc.* **2012**, *159*, H782–H786.

[5] Y. Meng, W. Song, H. Huang, Z. Ren, S. Y. Chen, S. L. Suib, *J. Am. Chem. Soc.* **2014**, *136*, 11452–11464.

[6] J. C. Hunter, *J. Solid State Chem.* **1981**, *39*, 142–147.

[7] L. Mao, D. Zhang, T. Sotomura, K. Nakatsu, N. Koshiba, T. Ohsaka, *Electrochim. Acta* **2003**, *48*, 1015–1021.

[8] a) J. A. Dawson, H. Chen, I. Tanaka, *ACS Appl. Mater. Interfaces* **2015**, *7*, 1726 – 1734; b) R. Yang, X. Lu, X. Huang, Z. Chen, X. Zhang, M. Xu, Q. Song, L. Zhu, *Appl. Catal. B* **2015**, *170 – 171*, 225 – 232; c) J. A. Dawson, I. Tanaka, *ACS Appl. Mater. Interfaces* **2014**, *6*, 17776 – 17784; d) F. Cheng, T. Zhang, Y. Zhang, J. Du, X. Han, J. Chen, *Angew. Chem. Int. Ed.* **2013**, *52*, 2474 – 2477; *Angew. Chem.* **2013**, *125*, 2534 – 2537.

[9] a) H. Wang, Z. Lu, S. Xu, D. Kong, J. J. Cha, G. Zheng, P. C. Hsu, K. Yan, D. Bradshaw, F. B. Prinz, Y. Cui, *Proc. Natl. Acad. Sci. USA* **2013**, *110*, 19701 – 19706; b) H. Wang, H. W. Lee, Y. Deng, Z. Lu, P. C. Hsu, Y. Liu, D. Lin, Y. Cui, *Nat. Commun.* **2015**, *6*, 7261; c) Y. Liu, H. Wang, D. Lin, C. Liu, P.-C. Hsu, W. Liu, W. Chen, Y. Cui, *Energy Environ. Sci.* **2015**, *8*, 1719 – 1724; d) Z. Lu, H. Wang, D. Kong, K. Yan, P. C. Hsu, G. Zheng, H. Yao, Z. Liang, X. Sun, Y. Cui, *Nat. Commun.* **2014**, *5*, 4345.

[10] Y. Xia, H. Wang, Q. Zhang, H. Nakamura, H. Noguchi, M. Yoshio, *J. Power Sources* **2007**, *166*, 485 – 491.

[11] a) Y. Gao, J. R. Dahn, *Solid State Ionics* **1996**, *84*, 33 – 40; b) M. R. Palacín, Y. Chabre, L. Dupont, M. Hervieu, P. Strobel, G. Rousse, C. Masquelier, G. G. Amatucci, J. M. Tarascon, *J. Electrochem. Soc.* **2000**, *147*, 845 – 853.

[12] M. Yoshio, H. Noguchi, H. Wang, X. Wang, *J. Power Sources* **2006**, *154*, 273 – 275.

[13] A. Damjanovic, D. B. Sepa, M. V. Vojnovic, *Electrochim. Acta* **1979**, *24*, 887 – 889.

[14] J. P. Brenet, *J. Power Sources* **1979**, *4*, 183 – 190.

[15] U. Maitra, B. S. Naidu, A. Govindaraj, C. N. R. Rao, *Proc. Natl. Acad. Sci. USA* **2013**, *110*, 11704 – 11707.

Received: March 22, 2016
Revised: May 10, 2016
Published online: June 2, 2016

